Geotech Geol Eng (2020) 38:1591–1603
https://doi.org/10.1007/s10706-019-01114-6

ORIGINAL PAPER

Discrete Element Numerical Simulation Method for Permeability Stress Sensitivity of Persistent Fractured Coal Samples

Cun Zhang · Zhaopeng Ren · Lei Zhang

Received: 25 June 2019 / Accepted: 25 October 2019 / Published online: 31 October 2019

Abstract The stress sensitivity of the persistent fracture and primary joint directly affect the stress and permeability of elastic and shear fracture coal samples in fluid–solid coupling simulation. Therefore, the method to select the parameters of the primary joints and persistent fracture affects the accuracy and reliability of the numerical simulation. This paper introduces the discrete element flow coupling simulation program based on the cubic law. The research on the relationship between flow rates and model parameters, including the mesh number, practice length, aperture, model size, and pressure difference, were performed. The fitting formulas of the flow rates and model parameters were obtained by numerical simulation. Based on the experimental study on the stress permeability of the elastic coal sample and the persistent fracture coal sample, the fluid–solid coupling simulation parameters selection method of the initial joint and persistent fracture is presented. The numerical simulation results with the calculation parameters under triaxial equi-compressive and deviatoric loads are in good agreement with the experimental results, indicating that the method herein can well simulate the relationship between the stress and permeability of the coal samples.

Keywords Persistent fracture · Discrete element method · Permeability · Stress sensitivity · Laboratory test

C. Zhang (✉) · Z. Ren
State Key Laboratory of Coal Resources and Safe Mining, China University of Mining and Technology, Beijing 100083, China
e-mail: cumt_zc@163.com

C. Zhang · Z. Ren
School of Energy and Mining Engineering, China University of Mining and Technology (Beijing), Beijing 100083, China

C. Zhang
State Key Laboratory Cultivation Base for Gas Geology and Gas Control, Henan Polytechnic University, Jiaozuo 454000, China

L. Zhang
Key Laboratory of Deep Coal Resource Ministry of Education of China, School of Mines, China University of Mining and Technology, Xuzhou 221116, Jiangsu, China

1 Introduction

The study on the stress sensitivity of coal seam is primarily based on oil and gas extraction; the stress models such as Palmer–Mansoori (P&M), Shi–Durucan (S&D), Cui–Bustin (C&B) and others were applied to predict the change in stress (or strain) permeability in Coalbed methane (CBM) exploitation (Cui and Bustin 2005; Palmer 2009; Zhang et al. 2016a; Shi and Durucan 2013). In these models, the strain changes due to different causes are summed. In addition, these models use a geomechanics

framework, which leads to more fundamental constants in the equations for permeability changes. In the P&M model, two separate equations are used to express (1) porosity change, (2) horizontal stress change, in terms of pore pressure change and matrix shrinkage. The S&D model is stress-based rather than strain-based. A theoretical clarification of the pore–volume compressibility issue has been provided by C&B model.

In addition to oil and gas exploitation, the stress sensitivity of coal and rock mass has been studied in many fields, such as coal and gas simultaneous extraction, and nuclear waste storage (Zhang et al. 2015; Xie et al. 2015; Ortiz et al. 2002; Marchand et al. 2008). The research methods of stress–fracture–permeability can be primarily divided into laboratory experiment and numerical simulation. The experimental study of stress permeability is relatively early; however, owing to the limitation of experimental equipment, the precision of the experiment is limited and the effects of fractures are considered less. Owing to the large influence of fracture on the permeability and its stress sensitivity, stress–fracture–permeability has been studied by many scholars (Yang et al. 2013; Xiao et al. 2014; Singh et al. 2015; Jafari et al. 2016). It is thought that such studies will be useful in identifying the limits of applicability of the well-known "cubic law," which is required for the precise calculation of discharge and/or aperture in any practical issues, and in further improving the theoretical/numerical models associated with fluid flow through a single fracture. Besides, many scholars have also studied the effect of fracture on coal and rock mass permeability including particle filling in the fractures and the roughness of the structure surface (Zou et al. 2013; Liu et al. 2014; Pan et al. 2010).

Currently, with the rapid development of computing technology, numerical methods are attracting more attention in the permeability study of fractured rock mass. The numerical modeling methodology of fractured rocks is based on reality, the fractures' complex geometry, and the interaction between the joints and rock blocks. The hybrid numerical discrete fracture network–distinct element method (DFN–DEM) and bonded particle (or grain)–distinct element method (BPM-DEM) model approach provides effective methods for calculating the mechanical properties of fractured rocks (Zhang et al. 2005; Min et al. 2004; Yao et al. 2015a; Baghbanan and Jing 2007; Zhang et al. 2019). The general steps of the numerical simulation are divided into (1) statistical description of fracture structure distribution characteristics of coal mass; (2) numerical simulation of the reconstruction; (3) modified reconstruction model; (4) application of the numerical model. However, in many cases, numerical simulation is performed for the numerical inversion of seepage under the condition of no stress. The numerical simulation of fluid–solid coupling is usually based on the finite element numerical simulation. Linear correlations between volumetric strain and permeability are observed from numerical results. The calculation of permeability uses the stress or strain and considers the effect of fracture less (Karacan et al. 2007; Zhang et al. 2016b; Whittles et al. 2006). When the shear and tensile failure occurred in the coal and rock mass, it will produce a large number of fractures, and obvious changes in its permeability and stress sensitivity (Tan and Konietzky 2019). With the further development of numerical simulation, the effect of stress and original joint parameters on permeability and fluid flow patterns in fractured rock masses is studied by DEM (Baghbanan and Jing 2008; Yao et al. 2015b). However, the original joint parameters and fracture parameters will be different. Therefore, in the fluid–solid coupling simulation of fractured rock mass, it is necessary to distinguish between the primary and the persistent fractures. Moreover, because of the limitations on numerical simulation, such as simplification and assumptions in the numerical model, many influencing factors cannot be studied with the numerical simulation. Thus, in such conditions, numerical modeling in conjunction with a limited number of targeted field measurements and plenty of laboratory experimentation can be used efficiently in assessing the impact of mining on a regional scale.

Herein, based on the experimental study on the stress permeability of the elastic coal sample and the plastic fracture coal sample, the numerical simulation of the stress–fracture–permeability of the fractured coal sample and elastic coal sample is studied based on the discrete element numerical simulation software, Universal Distinct Element Code (UDEC). The parameters selection method of the fractured coal samples is provided, which can well simulate the relationship between the stress and permeability of the coal samples.

2 Experimental Backgrounds

Effective stress σ_1 is used herein; it contains the axial stress σ_2, confining stress σ_3, and gas pressure P. When the axial stress is equal to the confining stress, the calculation formula of effective stress as follows:

$$\sigma_1 = (\sigma_2 + 2\sigma_3)/3 - P \quad (1)$$

The steady-state method for the permeability test is adopted herein. Specialized permeability apparatus, known as Gas Injection to Flush Methane Testing Apparatus (GIFMTA, as shown in Fig. 1), was used to test permeability. Detailed description of this apparatus and test methods can be found in Zhang et al. (2019). Equation (2) is the formula for gas permeability in the steady-state permeability test.

$$K = \frac{2P_0Q_0\mu L}{A(P_1^2 - P_2^2)} \quad (2)$$

where K is the gas permeability, md; A is the cross-sectional area of the coal samples, cm^2; L is the length of the coal sample, cm; P_0, P_1, P_2 are the upstream pressure, downstream pressure, and atmospheric pressure, respectively, MPa; μ is the viscosity of the gas, MPa s; Q_0 is the flow under the atmospheric pressure, cm^3/s.

The test samples are located in the 13-1 coal seam in the Huainan coal field. The average cover depth and thickness of the coal seams are 870 m and 4.03 m, respectively. The gas content and the largest gas pressure of the 13-1 coal seam are 8.78 m^3/t and 3.7 MPa, respectively. The original permeability of the 13-1 coal seam is 0.002 md and belongs to the outburst coal seam. Figure 2 shows the details of the Huainan coalfield location and the cross section of the various seams including the 13-1 coal seam. The physical and mechanical parameters of the coal samples are shown in Table 1; the coal proximate analysis and adsorption of the a and b constants determination results are shown in Table 2 (Zhang et al. 2018). The raw coal samples were used in this experiment and the sample sizes were ϕ100 mm × 50 mm and ϕ50 mm × 50 mm, as shown in Fig. 3. The shear test of the standard coal sample (ϕ 50 mm × 50 mm) were performed and the shear failure coal sample with the shear fracture plane

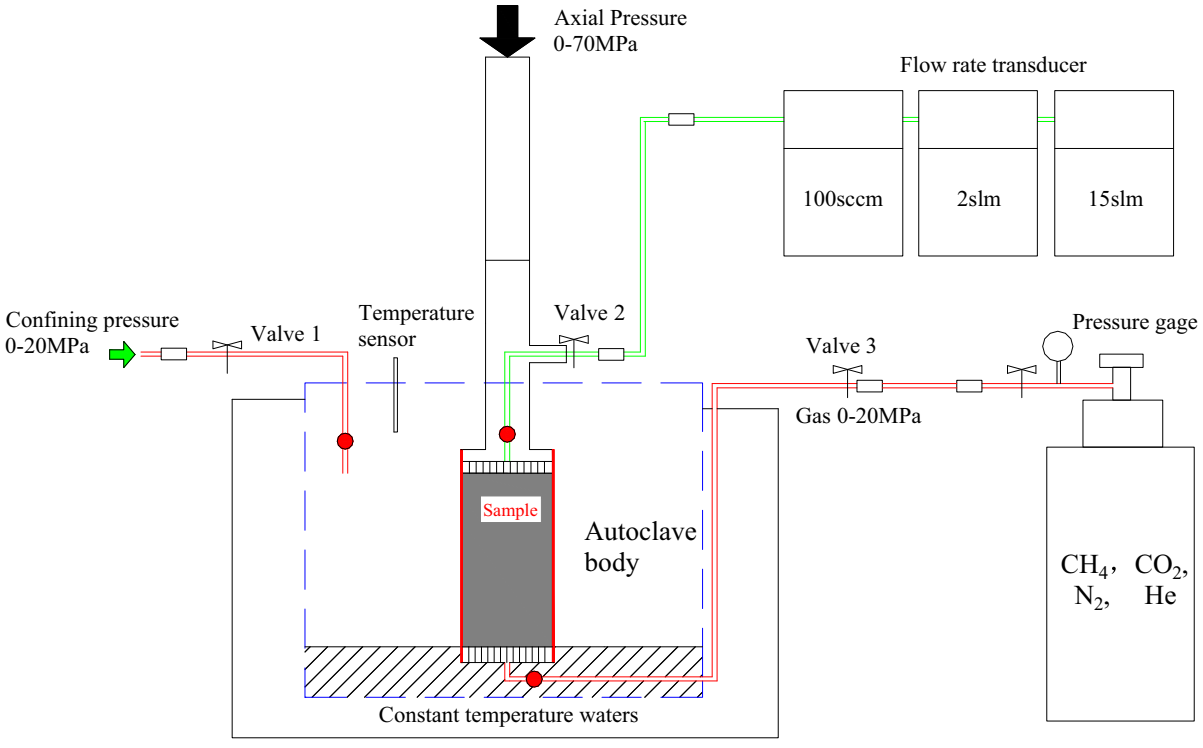

Fig. 1 Schematic diagram of the axial permeability test

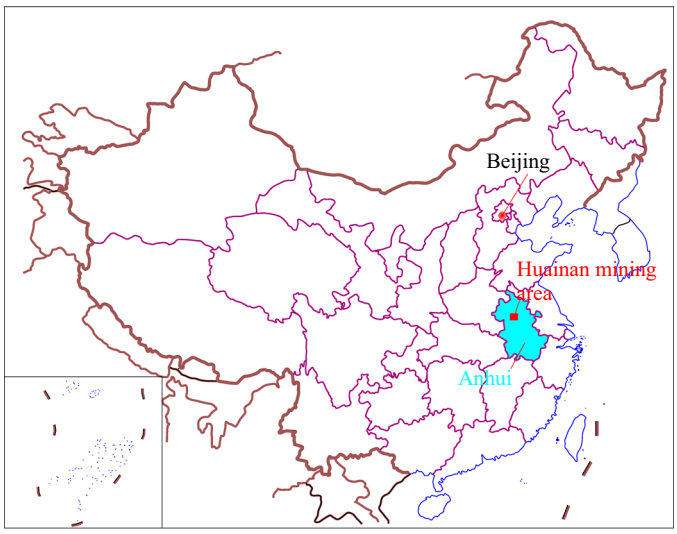

(a)

Columnar	Thickness (m)	Lithology
	3.49	Fine sandstone
	0.40	Coal line
	1.91	Mudstone
	5.67	Powder sandstone
	2.43	Sandy mudstone
	2.00	Mudstone
▲	4.58	13-1 Coal ▲
	4.32	Mudstone
	0.39	Coal line
	2.12	Fine sandstone
	10.4	Mudstone
	8.51	Powder sandstone
	8.61	Mudstone
	10.38	Sandy mudstone
	13.8	Powder sandstone
	6.44	Mudstone
●	1.24	11-2 Coal ●
	2.18	Mudstone
	1.43	Powder sandstone
	0.63	11-1 Coal
	3.87	Mudstone
	0.85	Sandy mudstone
	25.44	Powder sandstone

(b)

Fig. 2 Details of sampling location in Huainan coalfield, **a** Huainan coalfield location in China, and **b** the borehole diagram of the longwall face

Table 1 Coal proximate analysis and adsorption of a and b constants determination results

Mad (%)	Aad (%)	Vad (%)	St.ad (%)	TRD (g/cm^3)	a	b
1.70	18.28	29.75	0.10	1.67	8.521	2.133

Table 2 Physical and mechanical parameters of the coal samples

Elastic modulus, E_m	Poisson's ratio, ν_m	Cohesion, c_m	Tensile strength, t_m	Friction angle, φ_m	Compressive strength, σ_m
1.59 GPa	0.15	3.14 MPa	1.09 MPa	37.13°	15.98

Fig. 3 Raw coal samples

Fig. 4 Single fractured coal samples after shear test

perpendicular to the coal sample ends were selected for further experimental study, as shown in Fig. 4.

3 Discrete Element Numerical Simulation Method

3.1 Fluid–Solid Coupling Simulation Method

Herein, UDEC, a two-dimensional numerical program based on the DEM for discontinuum modeling, is used to simulate the response of a jointed rock mass subjected to static loading and fluid flow (Itasca Consulting Group, 2011). It uses a set of seeds to divide the space into polygonal Voronoi cells that typically have a relatively uniform grain size owing to the uniform distribution of their generating seeds (Nygards and Gudmundson 2002; Li et al. 2006). The particles were assumed to be impermeable, and the fluid was only allowed to flow through the connected contacts. The flow rate q within the planar contacts follows the cubic law, which can be written as

$$q = \frac{1}{12\mu} a^3 \frac{\Delta P}{l} \tag{3}$$

where k is the joint permeability, a is the contact hydraulic aperture, μ is the fluid viscosity, ΔP is the pressure difference between the two adjacent domains, and l is the length assigned to the contact between the domains. Further, the hydraulic aperture a is given by

$$a = a_0 - \sigma_n / k_n \tag{4}$$

where a_0 is the contact hydraulic aperture at zero normal stress, σ_{n} is the normal stress at the contact, and k_{n} is the contact normal interface stiffness. A minimum value, a_{res}, is assumed for the aperture, below which mechanical closure does not affect the contact permeability. Equations (3) and (4) show that the contact hydraulic aperture and contact normal interface stiffness significantly impact the relationship between permeability and stress in the DEM model for the stress flow coupling simulations. Thus, the two parameters above of the contact or fractures are the primary subject of test herein. In the flow calculation, the pore pressure is calculated by Eq. (5):

$$P = P_0 + K_w Q \frac{\Delta t}{V} - K_w \frac{\Delta V}{V_m} \tag{5}$$

where P is the new pore pressure of the domain, P_0 is the original pore pressure; K_w is the bulk modulus of the fluid; Q is the sum of the flow rate of the regional joint; $\Delta V = V - V_0$; $V_m = (V + V_0)/2$; V and V_0 are the new and original areas, respectively; Δt is the time step. The stress-–fracture flow coupling simulation can be performed using Eqs. (3)–(5). The entire flow process is shown in Fig. 5.

3.2 Steady-State Flow Algorithm

In this study, only the final steady-state condition is of interest. In this case, several simplifications can be performed to render the present algorithm highly efficient for many practical problems. The steady-state condition does not involve the domain volumes. Thus, these can be scaled to improve the convergence to the solution. A scheme that was found to produce good results consists of assigning a given domain a volume V that, when inserted in the time step expression above, leads to the same time step for all domains. The contribution of the change in domain volume to the pressure variation can be neglected, thus eliminating the influence of fluid stiffness in the mechanical time step, thus rendering it unnecessary to specify the fluid bulk modulus. Furthermore, as the steady-state condition is approached, the pressure variation in each fluid step becomes very small, allowing the execution of several fluid steps for each mechanical step without accuracy loss. An adaptive procedure that "triggers" the update of the mechanical quantities whenever the maximum increment of pressure in any domain exceeds some prescribed tolerance (for example, 1% of the maximum pressure) was implemented in the UDEC.

3.3 Joint Parameter Selection

The accuracy of the parameters in the numerical simulation directly determines the reliability of the numerical simulation. Mechanical parameters and fluid parameters are primarily considered in the fluid–solid coupling simulation; in addition to the physical parameters, the model size and mesh size affect the simulation accuracy. The full size of the laboratory equipment is used as the model size, which is sufficiently large to be constitutively valid. Thus, the model size is not discussed herein.

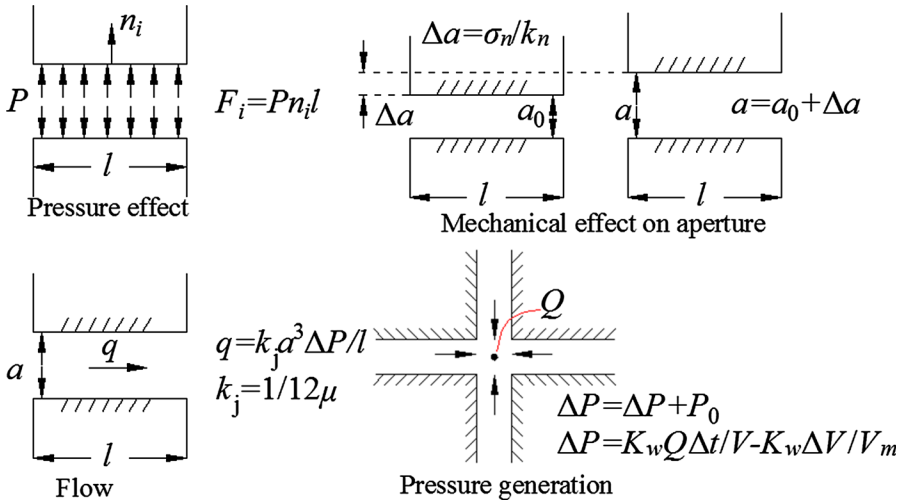

Fig. 5 Stress–fracture flow coupling simulation flow process

Practice size The UDEC uses a set of seeds to divide the space into polygonal Voronoi cells that typically have a relatively uniform distribution of grain sizes owing to the uniform distribution of their generating seeds, as shown in Fig. 6. The related research results show that the size of the irregular practice polygonal is less than 1/10 of the model size, thus resulting in little influence on the mechanical properties of coal and rock mass (Kazerani 2013). The particle assembly in the UDEC is generated arbitrarily. Thus, each simulation is run for five times with the same parameters and the results are averaged. It is noteworthy that the effect of the practice size on the fluid is significant, because the practice size directly determines the mesh density in the same model size, and the mesh density affects the seepage channel number.

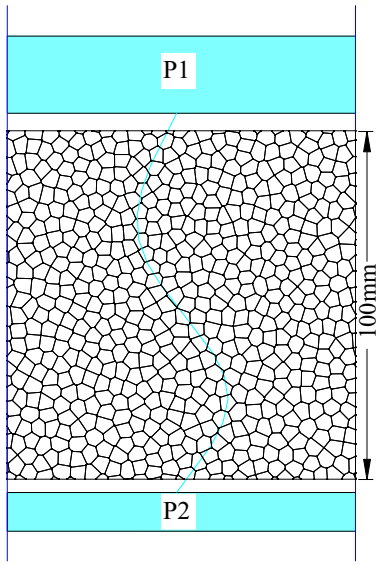

Fig. 6 Numerical model for seepage simulation

To study the influence of the practice number on the model flow, a 100 mm × 100 mm square model is established, as shown in Fig. 6. The practice lengths are 10 mm, 7 mm, 5 mm, 3 mm, and 1 mm. The flow simulation is divided into the vertical and horizontal direction without the stress state; the simulation results are listed in Table 3. The hydraulic aperture in the simulation is 2×10^{-5} m to accelerate the calculation speed. Q_h and Q_v represent the total flow rates of the horizontal and vertical flow rates, respectively.

For the same mesh number, the total horizontal and vertical flow rates are equal; the model can be regarded as an isotropic model. With the increase in the mesh number, Q_h and Q_v increase significantly. This is primarily due to the increase in the joint density that leads to the increase in the seepage channel, as shown in Fig. 7a, b. As shown from the figure, the

Table 3 Different meshes for numerical simulation of flow statistics

l_a (mm)	N	Q_h (m^2/s)	Q_v (m^2/s)
10	122	1.06×10^{-3}	1.06×10^{-3}
7	236	1.52×10^{-3}	1.53×10^{-3}
5	444	2.19×10^{-3}	2.18×10^{-3}
3	1188	3.74×10^{-3}	3.73×10^{-3}
1	10212	1.15×10^{-2}	1.15×10^{-2}

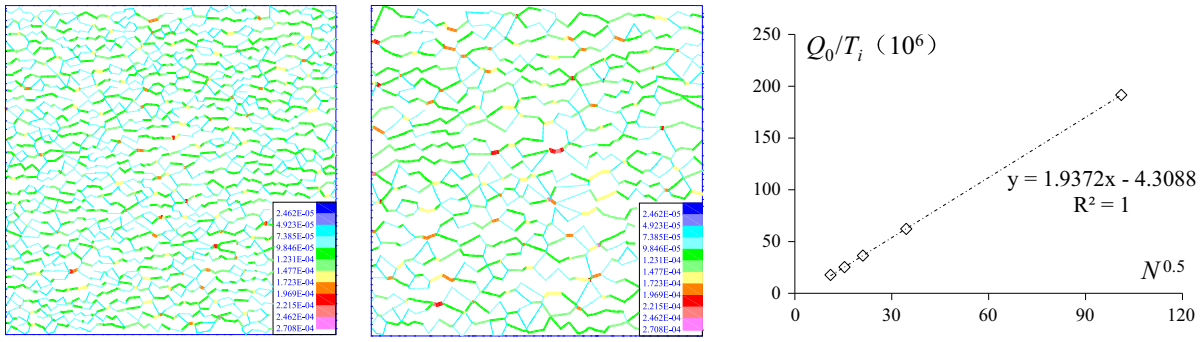

(a) N=1188 **(b)** N=444 **(c)**

Fig. 7 Seepage conditions of different meshes

number of channels of the 1188-mesh model is more than that of the 444-mesh model. Owing to the equal hydraulic aperture of each joint, according to Eq. (3), the flow rate of each channel is also equal. Thus, the total flow rates are proportional to the number of seepage channels (n), and n is equal to $N^{0.5}$. The permeability coefficient T_i in the simulation can be expressed as Eq. (6):

$$T_i = \frac{a^3}{12\mu} \tag{6}$$

Because ΔP and L remain unchanged, Q_0/T_i should be proportional to $N^{0.5}$. To verify the inference above, the curve of Q_0/T_i and $N^{0.5}$ is shown in Fig. 7c.

The linear correlation coefficient of the fitting curve $R^2 = 1$, confirms the inference above. The linear relationship between the mesh number and the flow rates of the 100 mm × 100 mm model can be expressed as Eq. (7):

$$\frac{Q_0}{T_i} = (1.937\sqrt{N} - 4.308) \times 10^6 \tag{7}$$

According to Eq. (7), the hydraulic aperture a can be calculated according to the permeability measured in the laboratory to determine the mesh number. However, owing to the general laboratory permeability test using the 100 mm × 50 mm or 50 mm × 50 mm model, the simulation analysis was conducted based on the two sizes; the simulation results are shown in Fig. 8.

As shown in Fig. 8, the fitting formulas of the different-size models are obviously different. In fact, the change in the model size arises from the change in the number of seepage channel n and the seepage length l. The seepage channel number is approximately equal to the length of the seepage section l_s divided by the irregular practice length l_a. The fitting curves of Q_0/T_i and l_s/l_a with various model sizes are shown in Fig. 9.

The fitting curve of the 100 mm × 100 mm model coincided with that of the 100 mm × 50 mm model. The gradient of the fitting curve with model size 50 mm × 50 mm is approximately 2 times that of the other two models. According to Eq. (3), this is due to the difference in the flow length l. In addition to l, the pressure difference ΔP and aperture a affect the fitting formula in Fig. 9. To further study the influence of ΔP and a on the fitting formula, this study uses the 100 mm × 100 mm model to simulate the seepage condition of ΔP = 1 MPa and $a = 4 \times 10^{-5}$ m; the simulation results are shown in Table 4.

As shown in Table 4, Q is proportional to a^3, i and inversely proportional to l; this is consistent with Eq. (3). To simulate all sizes of the laboratory permeability test samples, obtain the linear formula between Q and the model parameters including l, l_s, ΔP, a, and l_a must be obtained. All of the simulation data above were fitted to obtain the final fitting formula, as shown in Fig. 10. The parameter h in Fig. 10 is equal to $\Delta P/l$ and $n = l_s/l_a$.

$$\frac{Q_0}{T_i} = (0.954nh - 2.554) \times 10^6 \tag{8}$$

The initial joint aperture a_0 and joint stiffness k_n can be obtained with the laboratory measured Q, l, l_s, l_a under different stress states.

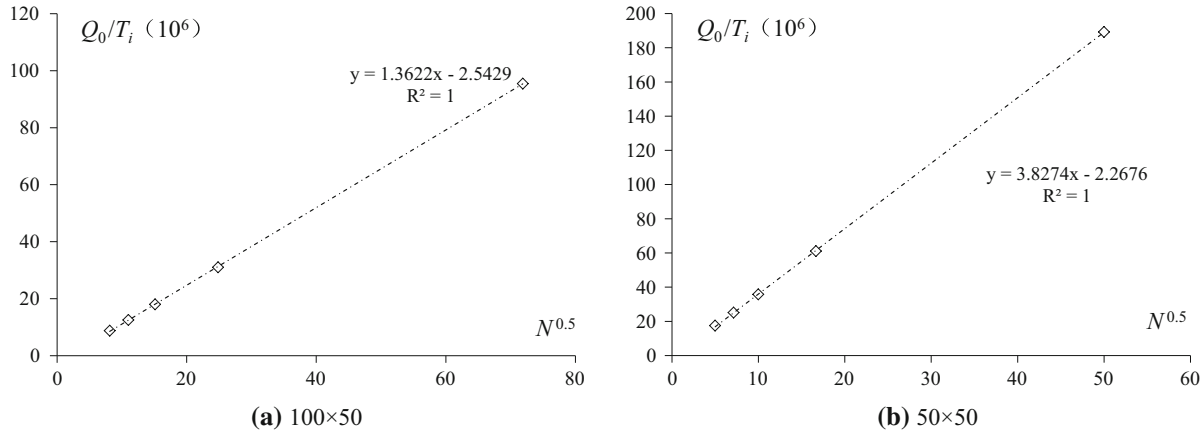

Fig. 8 Fitting curves of Q_0/T_i and l_s/l_a with various model sizes

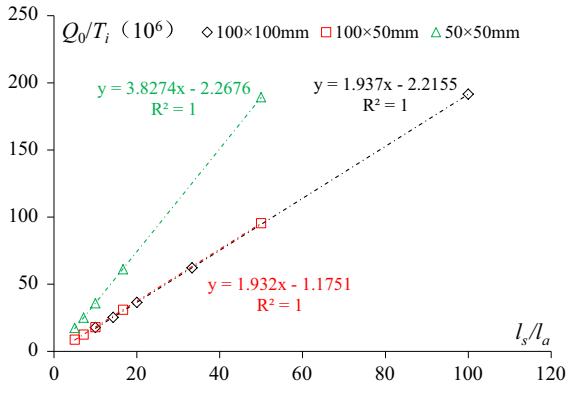

Fig. 9 Fitting curves of Q_0/T_i and l_s/l_a with various model sizes

4 Selection of Model Parameters and Verification

4.1 Selection and Verification of Joint Parameters

In many cases, reservoir rocks are often anisotropic in permeability, owing to the different pore or layering structures in different directions. However, after the coal sample is obtained, the seepage flows primarily along the fractures. Therefore, the axial seepage experiment date is primarily used to calculate the joint flow parameters of the isotropic model (Fig. 6). According to Darcy's law, Eq. (8) can be transformed into the permeability formula, k (m^2/MPa s).

$$k = \frac{(0.954nh - 2.554)(a_0 - \sigma_n/k_n)^3 \times 10^6}{12\mu h l_s} \tag{9}$$

To correspond with the laboratory research, the parameters are l = 0.05 m, l_s = 0.05 m, l_a= 0.002 m, ΔP = 0.2 MPa. The parameters above are introduced into Eq. (9) to obtain the permeability formula (md), stress, and joint normal stiffness.

$$k = 3.8677 \times (a_0 - \sigma_n/k_n)^3 \times 10^{16} \tag{10}$$

According to Eq. (10), a_0 and k_n can be obtained by fitting the measured data; the fitting results of the elastic coal samples are shown in Fig. 11 and Table 5.

Table 4 Seepage situation with different pressure differences and joint apertures

l (mm)	Different hydraulic aperture			Different pressure difference		
	$Q_0(m^2/s)/a = 2\times10^{-5}$	$Q_1(m^2/s)/a = 4\times10^{-5}$	Q_1/Q_0	$Q_1(m^2/s)/\Delta P$ = 0.2 MPa	$Q_3(m^2/s)/\Delta P$ = 1 MPa	Q_1/Q_3
10	1.06×10^{-3}	8.50×10^{-3}	8.00	1.06×10^{-3}	5.32×10^{-3}	0.20
7	1.52×10^{-3}	1.22×10^{-2}	8.00	1.52×10^{-3}	7.89×10^{-3}	0.20
5	2.19×10^{-3}	1.75×10^{-2}	8.00	2.19×10^{-3}	1.09×10^{-2}	0.20
3	3.74×10^{-3}	2.99×10^{-2}	8.00	3.74×10^{-3}	1.86×10^{-2}	0.20
1	1.15×10^{-2}	1.15×10^{-2}	8.00	1.15×10^{-2}	5.75×10^{-2}	0.20

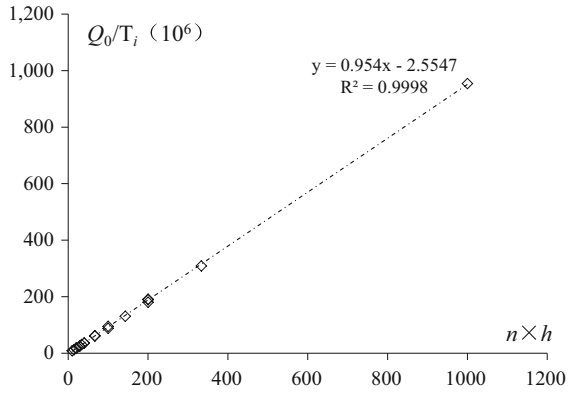

Fig. 10 Final fitting results with various parameters

As the stress increases during the simulation process, the hydraulic aperture will become negative according to Eq. (10). Therefore, a residual joint hydraulic aperture a_{res} is present to ensure that its value is always greater than 0. According to the laboratory measured curve (Fig. 11), when the effective stress exceeds 5 MPa, the change in permeability is very small. Thus, the maximum stress of the fitting curve is 6 MPa and the hydraulic aperture of 5 MPa is assumed to be the residual joint hydraulic aperture.

As shown in Fig. 11 and the corresponding Table 5, Eq. (10) can be well used to fit the measured results of the laboratory, and the fitting coefficient can reach more than 0.9. However, when the stress approached 6 MPa, the permeability of the fitted curve is significantly smaller than that of the experimental results. Therefore, it is necessary to set the residual joint hydraulic aperture to well simulate the laboratory stress seepage curve. Using the average value calculated in Table 5 to simulate the stress seepage of the elastic coal sample, the comparison between the numerical and measured results is shown in Fig. 12. As shown in the figure, the numerical simulation results are consistent with the experimental results. This indicates that the fluid–solid coupling parameters selected herein can be used for the numerical simulation of the stress seepage in elastic coal samples.

4.2 Selection and Verification of Fracture Parameters

After the seepage parameters selection of the elastic coal sample, it is necessary to select the fluid coupling parameters of the persistent fracture coal sample model (Fig. 13). It is obvious that the seepage of the persistent fracture does not accord with Eq. (10); however, it is consistent with the single fracture seepage formula, Eq. (3). Although the total flow of the persistent fracture coal sample includes the fracture flow and joint flow, the experimental results shows that the permeability of the elastic coal sample is relatively low, accounting for approximately 1–2% of the persistent fracture coal samples. Thus, the fluid coupling parameters of the persistent fracture can be directly obtained from fitting the seepage experimental data of the persistent fracture coal sample, using Eq. (11).

$$k = 1.6663 \times (a_0 - \sigma_n/k_n)^3 \times 10^{15} \tag{11}$$

According to Eq. (11), a_0 and k_n can be obtained by fitting the measured data; the fitting results of the elastic coal samples are shown in Fig. 14 and Table 6.

Compared with the fitting results of the elastic coal sample, the initial hydraulic aperture of the persistent fracture is much larger than that of the elastic coal sample by approximately 10 times. Meanwhile the normal stiffness is smaller than that of the elastic coal sample by one order of magnitude. Owing to the

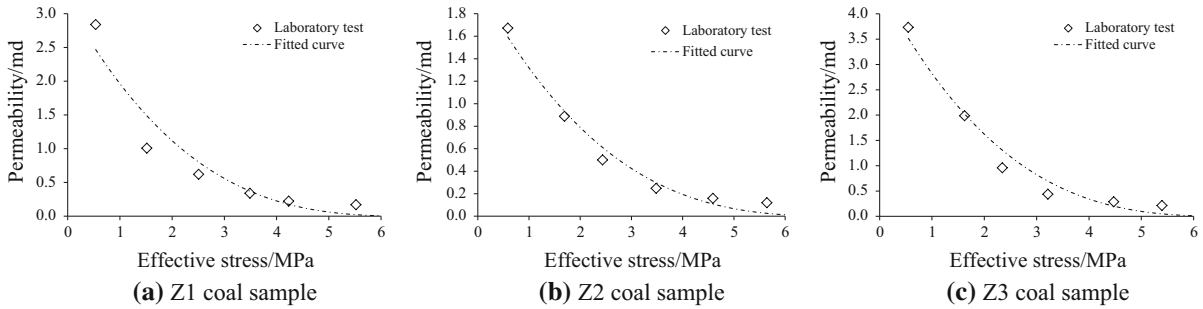

Fig. 11 Fitting curve of isotropic coal samples based on the cubic law

Table 5 Parameter fitting results of isotropic coal samples in DEM simulation

Coal sample ID	a_0 (m)	k_n (GPa)	a_{res} (m)	R^2
Z1	4.883×10^{-6}	1.421×10^{3}	6.61×10^{-7}	0.9658
Z2	4.337×10^{-6}	1.579×10^{3}	5.37×10^{-7}	0.9158
Z3	3.754×10^{-6}	1.959×10^{3}	6.91×10^{-7}	0.9766
Average value	4.325×10^{-6}	1.653×10^{3}	6.30×10^{-7}	

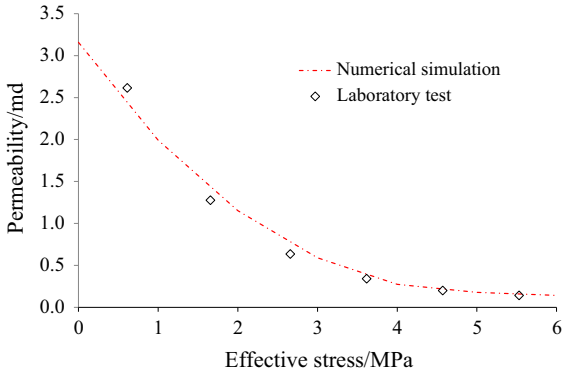

Fig. 12 Comparison results between laboratory test and numerical simulation of the isotropic coal samples

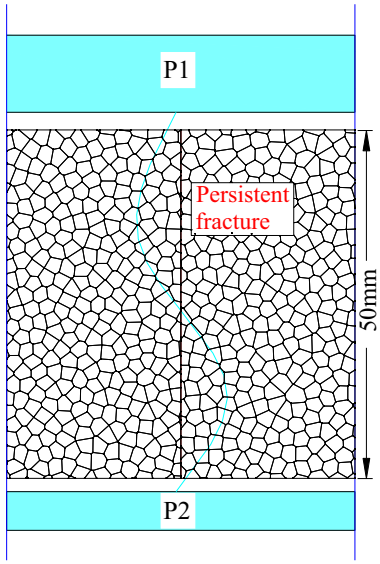

Fig. 13 Numerical model for persistent fracture coal sample seepage simulation

relatively high permeability of the fractured coal samples, the hydraulic aperture of 10 MPa is assumed to be the residual hydraulic aperture of the persistent fracture. Using the average value calculated in Table 7 to simulate the stress seepage of the persistent fracture coal sample, the comparison among the numerical results, S&D model and the measured results is shown in Fig. 15.

As shown in Fig. 15, the numerical simulation results are consistent with the experimental results and S&D model. This indicates that the fluid–solid coupling parameters selected herein can be used for the numerical simulation of the stress seepage in persistent fracture coal samples. To further verify the reliability of the model parameters, the seepage parameters obtained by the analysis above combined with the laboratory experiments were used to study the change in permeability under the deviatoric stress state. The range of the confining stress and axial stress is 1–5 MPa, the interval is 1 MPa, and the results of the numerical simulation and laboratory measurement are shown in Fig. 16.

As shown in Fig. 16, the numerical simulation results of the deviatoric loads are in good agreement with the experimental results, and the difference is relatively large only when the confining pressure is 1 MPa and the axial pressure is 5 MPa. The results of the numerical simulation and the measured results show that the sensitivity of the axial permeability to the confining stress is higher than that to the axial stress. This is primarily because the confining stress sensitivity of the persistent fracture aperture is greater than that of the axial stress, and the persistent fracture aperture directly determines the value of the axial permeability.

5 Conclusion

The fluid–solid coupling simulation of fractured coal and rock is beneficial to study the influence of fracture structure on the stress sensitivity of permeability. When shear and tensile failures occur in the coal and rock mass, a large number of fractures will be produced, as well as obvious changes in permeability and its stress sensitivity. Owing to the original joint parameters, the fracture parameters will be different. It

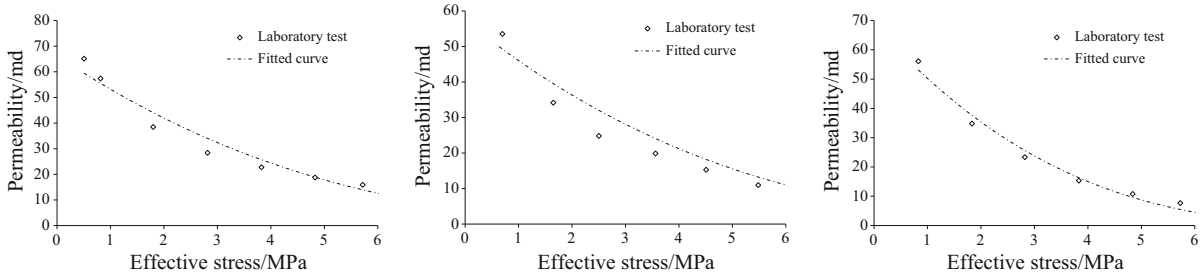

Fig. 14 Fitting curves of shear fracture coal samples based on the cubic law

Table 6 Parameter fitting results of persistent fracture in DEM simulation

Coal sample ID	a_0 (m)	k_n (GPa)	a_{res} (m)	R^2
S1	3.956×10^{-5}	3.588×10^{2}	1.170×10^{-5}	0.9500
S2	3.415×10^{-5}	4.134×10^{2}	0.996×10^{-5}	0.9359
S3	3.455×10^{-5}	2.914×10^{2}	0.023×10^{-5}	0.9766
Average value	3.609×10^{-5}	3.545×10^{2}	0.730×10^{-5}	

Table 7 UDEC calibrated parameters to represent the coal

E_m	1.59 GPa	v	0.15
k_{ne}/k_{nf}	1653/354.5 GPa/m	φ	37.13°
k_{se}/k_{sf}	600/130.7 GPa/m	t	2.09 MPa
c	2.84 MPa	d	2 mm

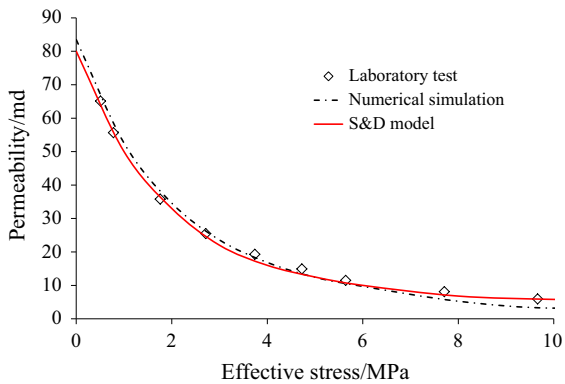

Fig. 15 Comparison results among laboratory test, S&D model and numerical simulation of the persistent fracture models under a static load

is necessary to distinguish between the primary joint and the persistent fractures in the fluid–solid coupling simulation. Moreover, because of the limitations in the numerical simulation, numerical modeling in conjunction with a limited number of targeted field measurements and plenty of laboratory experimentations can be used efficiently in assessing the impact of mining on a regional scale. Based on the experimental study on the stress permeability of the elastic coal sample and the plastic fracture coal sample, the numerical simulation of the stress–fracture–permeability of the fractured coal sample and elastic coal sample is studied. The main conclusions as follows:

1. This paper introduces the discrete element flow coupling simulation program based on the cubic law. The research on the relationship between the flow rates and model parameters, including the mesh number, practice length, aperture, model size, and pressure difference, were performed in Eq. (8).
2. According to Darcy's law, the fitting formulas [Eq. (9)] of the permeability and the model parameters were obtained by numerical simulation. Based on the experimental study on the stress permeability of the elastic coal sample and the persistent fracture coal sample, the parameters selection method of the initial joint and persistent fracture was presented: the fluid–solid coupling parameters, a_0 and k_n, can be obtained by fitting experimental measured data according to Eqs. (10) and (11).

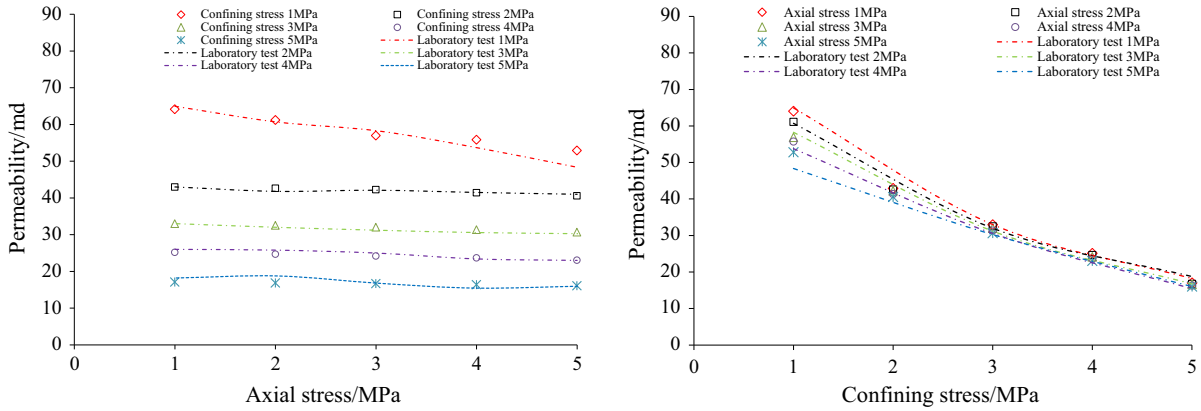

(a) Different confining pressures **(b)** Different axial pressures

Fig. 16 Comparison results between laboratory test and numerical simulation of the shear fracture models under a deviatoric load

3. The numerical simulation results with the calculation parameters under triaxial equi-compressive and deviatoric loads are in good agreement with the experimental results (The average error is less than 3% in test range), indicating that the method herein can well simulate the relationship between the stress and permeability of the coal samples.

Acknowledgements Financial support for this work was provided by Beijing Natural Science Foundation (8184082), the National Natural Science Foundation of China (Nos. 51874281, 51704274), the Open Fund of State Key Laboratory of Coal Resources and Safe Mining (No. SKLCRSM19KFA17), the State Key Laboratory Cultivation Base for Gas Geology and Gas Control (Henan Polytechnic University) (WS2019A05) and the Yue Qi Distinguished Scholar Project, China University of Mining and Technology, Beijing.

References

Baghbanan A, Jing L (2007) Hydraulic properties of fractured rock masses with correlated fracture length and aperture. Int J Rock Mech Min Sci 44(5):704–719

Baghbanan A, Jing L (2008) Stress effects on permeability in a fractured rock mass with correlated fracture length and aperture. Int J Rock Mech Min Sci 45(8):1320–1334

Cui X, Bustin RM (2005) Volumetric strain associated with methane desorption and its impact on coalbed gas production from deep coal seams. Aapg Bulletin 89(9):1181–1202

Itasca Consulting Group Inc (2011) UDEC: universal distinct element code, version 5.0. ICG, Minneapolis

Jafari S, Pouladi B, Sharifi M, Shabankareian B, Moraveji MK (2016) Experimental and simulation study of gas diffusion effect during gas injection into naturally fractured reservoirs. J Nat Gas Sci Eng 33:438–447

Karacan CÖ, Esterhuizen GS, Schatzel SJ, Diamond WP (2007) Reservoir simulation-based modeling for characterizing longwall methane emissions and gob gas venthole production. Int J Coal Geol 71(2–3):225–245

Kazerani T (2013) Effect of micromechanical parameters of microstructure on compressive and tensile failure process of rock. Int J Rock Mech Min Sci 64(6):44–55

Li H, Li K, Subhash G, Kecskes LJ, Dowding RJ (2006) Micromechanical modeling of tungsten-based bulk metallic glass matrix composites. Mater Sci Eng, A 429:115–123

Liu J, Li JL, Hu J, Cai J, Zhao ZY (2014) Comparative analysis of multiple factors affecting seepage flow of splitting sandstone with fillers or non-fillers. Rock Soil Mech 35(8):2163–2170

Marchand E, Clément F, Roberts JE, Pépin G (2008) Deterministic sensitivity analysis for a model for flow in porous media. Adv Water Resour 31(8):1025–1037

Min KB, Rutqvist J, Tsang CF, Jing L (2004) Stress-dependent permeability of fractured rock masses: a numerical study. Int J Rock Mech Min Sci 41(7):1191–1210

Nygards M, Gudmundson P (2002) Micromechanical modeling of ferritic/pearlitic steels. Mater Sci Eng, A 325:435–443

Ortiz L, Volckaert G, Mallants D (2002) Gas generation and migration in boom clay, a potential host rock formation for nuclear waste storage. Eng Geol 64(2):287–296

Palmer I (2009) Permeability changes in coal: analytical modeling. Int J Coal Geol 77(1):119–126

Pan Z, Connell LD, Camilleri M (2010) Laboratory characterisation of coal reservoir permeability for primary and enhanced coalbed methane recovery. Int J Coal Geol 82(3–4):252–261

Shi JQ, Durucan S (2013) Exponential growth in san juan basin fruitland coalbed permeability with reservoir drawdown? Model match and new insights. SPE Reserv Eval Eng 13(6):914–925

Singh KK, Singh DN, Ranjith PG (2015) Laboratory simulation of flow through single fractured granite. Rock Mech Rock Eng 48(3):987–1000

Tan X, Konietzky H (2019) Numerical simulation of permeability evolution during progressive failure of Aue granite at the grain scale level. Comput Geotech 112:185–196

Whittles DN, Lowndes IS, Kingman SW, Yates C, Jobling S (2006) Influence of geotechnical factors on gas flow experienced in a UK longwall coal mine panel. Int J Rock Mech Min Sci 43(3):369–387

Xiao W, Xia C, Deng R (2014) Advances in development of coupled stress-flow test system for rock joints. Chin J Rock Mechan Eng 33:3456–3465

Xie H, Jing X, Gao M, Ru Z, Zhou H, Feng G et al (2015) Theoretical and experimental validation of mining-enhanced permeability for simultaneous exploitation of coal and gas. Environ Earth Sci 73(10):5951–5962

Yang JB, Feng XT, Pan PZ (2013) Experimental study of permeability characteristics of single rock fracture considering stress history. Rock Soil Mech 34(6):1629–1635

Yao C, Jiang QH, Shao JF (2015a) A numerical analysis of permeability evolution in rocks with multiple fractures. Transp Porous Med 108(2):289–311

Yao C, Jiang Q, Shao J, Zhou C (2015b) Modelling of hydro-mechanical coupling and transport in densely fractured rock mass. Eur J Environ Civ Eng 19(5):521–538

Zhang KS, Wu MS, Feng R (2005) Simulation of microplasticity-induced deformation in uniaxially strained ceramics by 3-D Voronoi polycrystal modeling. Int J Plast 21(4):801–834

Zhang C, Tu S, Bai Q, Yang G, Zhang L (2015) Evaluating pressure-relief mining performances based on surface gas venthole extraction data in longwall coal mines. J Nat Gas Sci Eng 24:431–440

Zhang C, Tu S, Zhang L, Wang F, Bai Q, T H (2016a) The numerical simulation of permeability rules in protective seam mining. Int J Oil Gas Coal Technol 13(3):243–259

Zhang C, Tu S, Zhang L, Chen M (2016b) A study on effect of seepage direction on permeability stress test. Arab J Sci Eng 41(11):4583–4596

Zhang C, Zhang L, Zhao Y, Wang W (2018) Experimental study of stress–permeability behavior of single persistent fractured coal samples in the fractured zone. J Geophys Eng 15(5):2159–2170

Zhang C, Zhang L, Wang W (2019) The axial and radial permeability testing of coal under cyclic loading and unloading. Arab J Geosci 12(11):371–390

Zou L, Tarasov BG, Dyskin AV, Adhikary DP, Pasternak E, Xu W (2013) Physical modelling of stress-dependent permeability in fractured rocks. Rock Mech Rock Eng 46(1):67–81